Theoretical and Experimental Comparisons of the Self-pressurization in a Cryogenic Storage Tank for IOT Application

Juan Fu[(⊠)] and Jingchao Wang

China Electronic System Engineering Company, Beijing, China
fujuan0702@163.com

Abstract. The application of satellite technology in the Internet of Things (IOT) can just make up for the defects of the ground system for its wide coverage and anti-damage. More and more satellites will participate in IOT. Due to the environmental protection exhaust and high specific impulse of cryogenic propellants like liquid hydrogen and liquid oxygen, they will play an important role in satellite applications. Cryogenic liquid storage is difficult and self-pressurization phenomenon often occurs. Pressure rise prediction with high accurate is necessary when designing tank for storage. Numerical calculation of computational fluid dynamic model and experiments are always time and financial consuming. A theoretical thermal diffusion model is investigated in the paper by using a concentration parameter model in the vapor and a one-dimensional heat conduction model in the liquid. The validation of the predictive capability is conducted by comparing the predictions with experimental data. Favorable agreement is found for both the experimental cylindrical and oblate spheroidal tanks. The effect of fill level and tank size is also studied.

Keywords: Internet of Things (IOT) · Self-pressurization phenomenon · Cryogenic liquid · Theoretical thermal diffusion model

1 Introduction

The Internet of Things (IOT) is a universal network that will timely obtain, transmit, and intelligently process information such as wide area geography, environment, space, and mobile objects to achieve a comprehensive interconnection of wide areas. The inability of The conventional ground equipment and systems is failure to provide high-density, full-coverage real-time data acquisition and data transmission services for large or specific areas. It results in the lack of the necessary remote sensing and communication network support for IOT applications in these areas. Further, in disaster conditions, ground infrastructure is easily destroyed, and emergency network construction is inconvenient, so the application of the IOT and disaster emergency monitoring are greatly limited. The application of satellite technology in the IOT can just make up for the defects of the ground system, its coverage is wide and the system is persistent. The flexibility of

the space-based network determines that it will play a necessary and irreplaceable role in the IOT industry.

More and more satellites will participate in the IOT system. The propellant is needed for rocket launch and satellite attitude and orbit control. Due to the Environmental Protection exhaust and High specific impulse of cryogenic propellants like liquid hydrogen and liquid oxygen, they will play an important role in satellite applications. However, cryogenic liquid storage is difficult because the heat leak is inevitable. Thus phase change happens and the tank pressure will rise regularly. It is important to predict the pressure rise trend for the pressure control and the proper tank design.

Many methods have been developed by investigators by considering time and financial consuming besides prediction accuracy. Pressure rise tendency is often compared with experimental data to judge the methods. One-dimensional methods were used in the primary quickly tank design for its low time and financial consuming with acceptable prediction accuracy. These models often ignored heat transportation in fluid or vapor part. A homogeneous thermodynamic analysis [1] was studied assuming the energy rise rate was the same in the tank fluid. Thus, the model prediction was not well matched with the experimental data. Hochstein et al. [2] considered the transport only in liquid and compared the tendency with experiment [3]. Prediction accuracy depended on the heat location and gravity. The capability of the model proposed by Amirkhanyan and Cherkasov [4] was influenced by tank fill level. Further, CFD models were developed for computer technology development. Thermal stratification and phase change at the interface was considered in the CFD model to forecast the pressure rise [5, 6]. Results were evaluated with test data [7]. Reasonable forecast obtained only for low liquid fraction case. Other CFD models were investigated by changing condition at the interface [8] or including transport in both liquid and vapor parts [9]. The later was validated with experiment and accuracy depended on the gravity and heat leak.

Here, the self-pressurization in a closed cryogenic vessel is predicted by employing the conductivity model in liquid and lumped model for vapor phase. It is a time saving method to accurately predict the pressure rise in the enclosure tank compared with the CFD method and experiments. The performance is assessed by comparing the computing predictions with experimental self-pressurization data.

2   Mathematical Model

The partly filled cryogenic vessel is schematically illustrated in Fig. 1. The tank volume V_T is divided by the interface of the two phases into liquid volume V_L and gas volume V. Total heat leak of Q is imposed on the tank wall. Therefore, the external heat loads delivered through the dry and wetted parts of the tank are noted as Q_L and Q_V, respectively. Only liquid vapor exists in the gas part. Under these conditions, one can assume that the pressure in the vessel is unambiguously related via the saturation curve to the temperature on the interface T_S; because the pressure drops in the gas phase are small, the pressure p_V and temperature T_S may be assumed to be functions of time alone.

The governing formulas of mass, momentum, and energy are

$$\frac{\partial \rho}{\partial t} + \nabla \cdot \left(\rho \vec{V} \right) = 0 \tag{1}$$
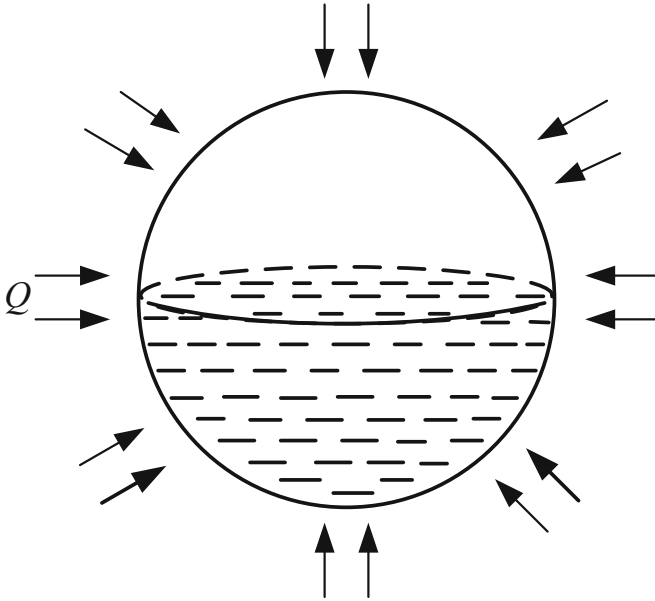
Fig. 1. Schematic diagram of the cryogenic vessel

$$\frac{\partial\left(\rho\vec{V}\right)}{\partial t} + \nabla\cdot\left(\rho\vec{V}\vec{V}\right) = -\nabla p - \nabla\cdot(S) + \rho\vec{g} \tag{2}$$

$$\frac{\partial(\rho E)}{\partial t} + \nabla\cdot\left(\vec{V}(\rho E + p)\right) = -\nabla\cdot\left(S\cdot\vec{V}\right) + \nabla\cdot(\lambda\nabla T) \tag{3}$$

Where the compressive stress $S = -\mu\left(\nabla\vec{V} + \nabla\vec{V}^{T}\right) + \left[\left(\frac{2}{3}\mu - \zeta\right)\nabla\cdot\vec{V}\right]\mathbf{I}$, ρ is the fluid density, $\vec{V}$ is the fluid speed vector, p is the tank pressure, $\vec{g}$ is the acceleration of gravity, $E = h - \frac{p}{\rho} + \frac{V^2}{2} = u + \frac{V^2}{2}$ is the fluid energy per unit mass, h and u are the fluid specific enthalpy and specific internal energy respectively. λ is the fluid Thermal conductivity.

The mass rate at the interface between the two phases resulted from the evaporation or condensation is

$$j = \rho_{\mathrm{L}}(\mathbf{V_L} - \mathbf{V_I})\cdot\hat{n} = \rho_{\mathrm{V}}(\mathbf{V_V} - \mathbf{V_I})\cdot\hat{n} \tag{4}$$

when $\hat{n}$ pointing the liquid is positive, $\mathbf{V_L}$, $\mathbf{V_V}$, $\mathbf{V_I}$ is the speed vector of liquid, vapor and interface, respectively.

In the non-thermodynamic equilibrium state, the temperature appears at the intersection of two phases is not continuous, assuming that the interface temperature is the saturation temperature of the system. According to Fourier's law, the difference in heat flow density between the two sides of the interface is obtained:

$$\|q_s\| = \left[\left(-\lambda_{\mathrm{L}}\frac{\partial T}{\partial n}\right)\bigg|_{\mathrm{L}} - \left(-\lambda_{\mathrm{V}}\frac{\partial T}{\partial n}\right)\bigg|_{\mathrm{V}}\right]\mathbf{n} \tag{5}$$

n is the unit normal vector pointing to the vapor. Phase change mass flow caused by heat density is

$$j = \frac{q_s}{L} \tag{6}$$

The positive j means evaporation, negative number means condensation. The unit is kg/(m^2·s). L is the latent heat of vaporization.

The boundary conditions are as follows. The heat from the environment is $\dot{Q}$, Assuming the tank area is A, the heat flux $q = \dot{Q}/A$. At the sidewalls and interface, no slip boundary conditions are chosen. The initial condition is

$$\vec{V} = 0$$
$$T = T_0$$
$$P_0 = P_{sat}(T_0) \tag{7}$$

The initial status is the saturation state.

The control equation is nonlinear, it is difficult to solve it directly. Therefore, some assumptions are generally added to predict the pressure. The earliest applied computational model was the Uniform Thermodynamic Model [1]. The model assumes that the temperature in the vapor and liquid parts is the same, the pressure is equal to the saturated vapor pressure corresponding to the system temperature, the fluid is not pressurized, and the fluid properties do not change with the temperature. The model will be used for comparative analysis with a thermal diffusion model (TDM) combined with a gas concentration parameter model and a liquid heat conduction model proposed in this paper. The TDM takes into account the different temperature change rates of gas and liquid phase, and the two phases are mathematically modeled. The coupling solution is obtained by mass and energy transmission at the interface.

2.1 Gas Concentration Parameter Model

Mass Control Formular. Due to the volume of the tank and the total mass of the fluid medium are unchanged, there are:

$$\begin{aligned}
\frac{\mathrm{d}}{\mathrm{d}t}(\rho_V V) &= \frac{\mathrm{d}}{\mathrm{d}t}\left[m_p - \rho_L(V_T - V)\right] \\
&= \frac{\mathrm{d}}{\mathrm{d}t}(\rho_L(V - V_T)) = \frac{\mathrm{d}}{\mathrm{d}t}(\rho_L V) \\
&= J
\end{aligned} \tag{8}$$

Where $J = jA_I$ the phase transition rate (kg/s), A_I is the interface area, m_p is the total mass of the gas and liquid in the vessel, V is the gas phase volume, V_T is he total volume of the tank. ρ_V and ρ_L are the gas phase density and liquid phase density respectively. Ignoring the change in liquid density, the above formula is transferred to

$$\frac{\mathrm{d}V}{\mathrm{d}t} = \frac{J}{\rho_L} \tag{9}$$

The heat required for phase transition evaporation is the difference in heat flow at the interface:

$$LJ = \dot{Q}_{IL} - \dot{Q}_{IV} \Rightarrow \dot{Q}_{IV} = \dot{Q}_{IL} - LJ \tag{10}$$

Where $\dot{Q}_{IL} = \int_I (-\lambda_L \nabla T_L) \cdot \vec{n} dS$ is the heat flow on the liquid side of the interface, $\vec{n}$ refers to the unit vector perpendicular to the interface pointing to the gas phase, $\dot{Q}_{IV} = \int_I (-\lambda_V \nabla T_V) \cdot \vec{n} dS$ is the heat flow on the gas side of the interface.

Ignoring changes in liquid density, the gas volume in Eq. (8) is

$$V = V_0 \frac{\rho_L - \rho_{V,0}}{\rho_L - \rho_V} = V_0 \left(1 + \frac{\rho_V - \rho_{V,0}}{\rho_L - \rho_V}\right) \tag{11}$$

Where V_0 the initial volume of the gas, $\rho_{V,0}$ is the initial density. In the case where the gas density change value is very small relative to the density difference between the liquid and the gas density, the gas density is very close to the initial value.

The gas density obtained from the gas state equation is:

$$\rho_V = \frac{p_V}{RT} \tag{12}$$

Where R is gas constant, $R = R_M / M$, the ratio of the general gas constant R_M to the molar mass of the gas M.

Assuming that the gas phase is saturated, the temperature T is the saturation temperature T_S corresponding to the tank pressure P_V, $T = T_S$, T_S and P_V are satisfying the saturated vapor pressure:

$$\frac{1}{T_S} = \frac{1}{T_B} - \frac{R}{L} \ln\left(\frac{p_V}{p_B}\right) \tag{13}$$

T_B and p_B are the value of a reference saturation state.

Energy Control Formular. The gas energy change is:

$$\frac{d}{dt}(\rho_V V u) = \dot{Q}_V + \dot{Q}_{IV} + J\left(u + \frac{p_V}{\rho_V}\right) - p_V \frac{dV}{dt} \tag{14}$$

$\dot{Q}_V$ is the heat flow into the gas phase transmitted through the tank wall of gas part, Ju is the internal energy changes caused by evaporation, $J p_V / \rho_V$ is the pressure work due to changes in evaporation; $-p_V dV / dt$ is the External work for volume changes.

Expanding Eq. (14) and Substituting Eq. (8)–(10) into Eq. (14), Ju is eliminated, the following formula is obtained:

$$\rho_V V \frac{du}{dt} + J\left[L - p_V \left(\frac{1}{\rho_V} - \frac{1}{\rho_L}\right)\right] = \dot{Q}_V + \dot{Q}_{IL} \tag{15}$$

Further, substituting $u = c_V T_S$ and $J = \frac{d}{dt}(\rho_V V)$ into Eq. (15), there is

$$\left\{\rho_V V c_V + \frac{\partial}{\partial T_S}(\rho_V V)\left[L - p_V\left(\frac{1}{\rho_V} - \frac{1}{\rho_L}\right)\right]\right\} \frac{dT_S}{dt} = \dot{Q}_V + \dot{Q}_{IL} \tag{16}$$

It will be abbreviated as:

$$\frac{dT_S}{dt} = B(\dot{Q}_V + \dot{Q}_{IL}) \tag{17}$$

Where B is the function of pressure.

$$B = \left\{ \rho_V V c_V + \frac{\partial}{\partial T_S}(\rho_V V)\left[L - p_V\left(\frac{1}{\rho_V} - \frac{1}{\rho_L}\right)\right]\right\}^{-1} \tag{18}$$

Combing Eq. (8)–(13), there are

$$\frac{\partial p_V}{\partial T_S} = \frac{L p_V}{R T_S^2}$$

$$\frac{\partial}{\partial T_S}(\rho_V V) = \frac{\rho_V \rho_L V}{\rho_L - \rho_V}\left(\frac{1}{R T_S^2} - \frac{1}{T_S}\right) \tag{19}$$

Then Eq. (18) is changed into

$$B = \left\{ \rho_V V c_V + \frac{\rho_V \rho_L V}{\rho_L - \rho_V}\left(\frac{1}{R T_S^2} - \frac{1}{T_S}\right)\left[L - p_V\left(\frac{1}{\rho_V} - \frac{1}{\rho_L}\right)\right]\right\}^{-1} \tag{20}$$

By calculating Eq. (16), the saturation temperature T_S of the gas is obtained. Since the temperature and pressure satisfy the saturation vapor pressure equation, the pressure change p_V in the vessel can be calculated. Solving Eq. (16) the $\dot{Q}_{IL}$ needs to be known. $\dot{Q}_{IL}$ will be given by the temperature field calculation of the liquid phase. The Coupling calculation of gas and liquid phase is through $\dot{Q}_{IL}$.

2.2 Liquid Thermal Conductivity Model

There are two views on the influence of convection on the temperature field. First, convection is considered to be a forced agitation that can reduce temperature heterogeneity and therefore reduce temperature stratification. The second is that natural convection is an upward fluctuation of the heat flow. Therefore, when heat is transported from different sides into the liquid body, convection will cause overheating of the top liquid layer, thereby increasing the temperature stratification. By numerical simulation of the liquid heat leakage in the vertical cylindrical tank, the results are compared with the thermal conductivity problems, and it is found that the influence of convection on temperature is actually a combination of the above two views. Due to convection, the heat on the wall and bottom is transported into the liquid body to reduce the uneven temperature distribution. On the other hand, convection increases the temperature of the top boundary of the liquid. The temperature field is formed owing to thermal conductivity and convection. Because of the buoyancy, liquid near the heated wall moves up. When it reaches the top surface, it turns towards the center and finally reaches at the boottom. Thus circulation flow is determines in the liquid. Finally thermal stratification is formed, which means

the temperature is a function of the height of the tank. This is observed by both the experiments [10] and CFD results [11, 12].

Therefore, for the specificity of the convection effect, the following assumptions are made for the calculation [4]: (1) The heat entering the liquid through the wall surface is evenly distributed in the entire liquid volume under convection, (2) The heat entering the interior of the liquid through the top interface is diffused into the liquid in the form of thermal conductivity. The vertical thermal conductivity is the fluid thermal conductivity coefficient, and the horizontal thermal conductivity coefficient is infinity, that is, the liquid at different heights. The temperature is the same in the horizontal direction. Based on the above assumptions, a one-dimensional heat conduction model of liquid is obtained.

$$\rho_L c_L A \frac{\partial T}{\partial t} = \lambda_L \frac{\partial}{\partial z}\left(A \frac{\partial T}{\partial z}\right) + A \frac{\dot{Q}_L}{V_L}$$

$$\left.\frac{\partial T}{\partial z}\right|_{z=0} = 0, \quad \left.\lambda_L\left(A \frac{\partial T}{\partial z}\right)\right|_{z=H_L} = \dot{Q}_{IL} \tag{21}$$

Where A is the heat transfer cross-sectional area at the height z of the liquid surface, H_L is the height of the liquid surface, $\dot{Q}_L$ is the heat flow into the liquid, $\dot{Q}_L / V_L$ is equivalent to heat source density. The pressure change trend of the tank can be calculated by using the temperature value calculated by the liquid thermal conductivity model and the heat transfer at the interface as the boundary condition of the gas phase change.

3   Result and Discussion

The results obtained using the foregoing thermal diffusion model (TDM) for calculations under the experimental conditions of [13] are given in Fig. 2. The experimental data were obtained in a tank of 6.75 L with liquid nitrogen for different fill levels of different external heat fluxes. A thermodynamic method with no thermal stratification is also used for the comparison. Relevant thermodynamic properties of the fluid used in the calculation model are listed in Table 1.

Table 1. Thermodynamic properties of liquid nitrogen

Symbol	Property	Value
ρ_L	Liquid density	807.7 kg/m^3
c_L	Liquid specific heat at constant volume	2041.5 J/kg K
c_V	Vapor specific heat at constant volume	1040.67 J/kg K
λ_L	Liquid thermal conductivity	0.14657 W/m K
L	Latent heat	198300 J/kg

One can see that the use of Eq. (21) instead of the condition of the absence of thermal stratification in liquid results in a considerable reduction of discrepancy between theory
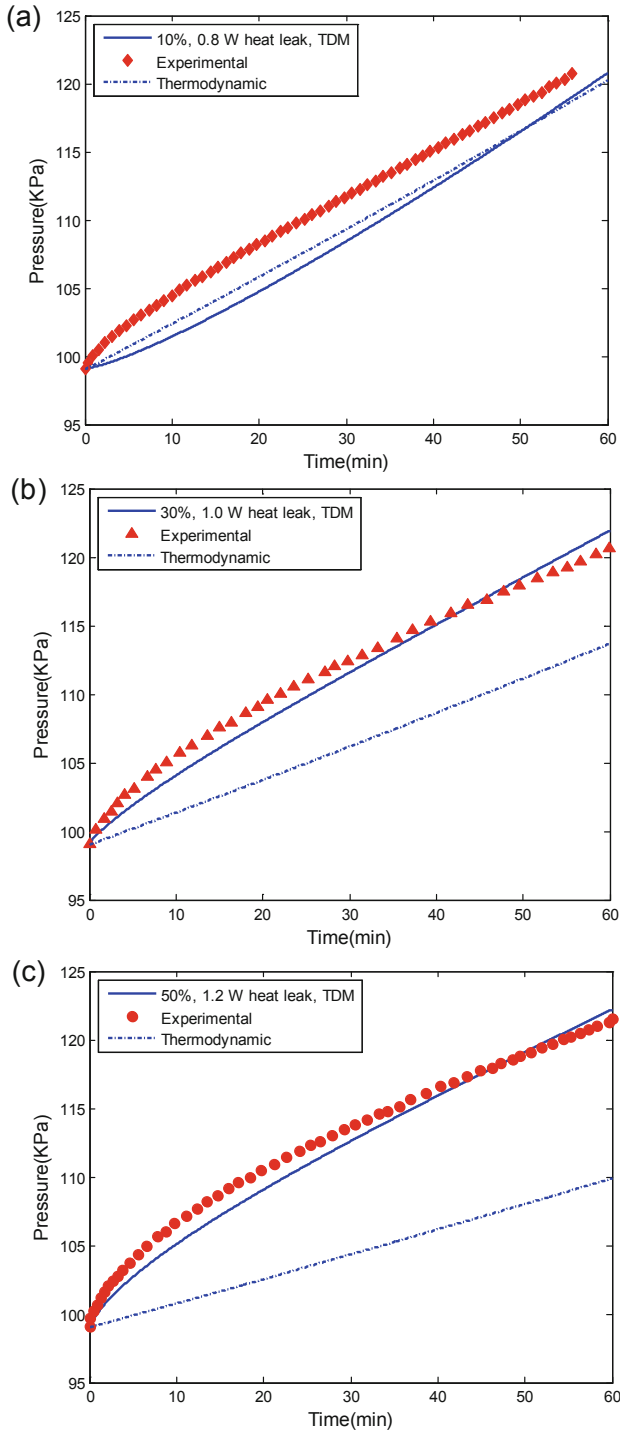
Fig. 2. Comparison of TDM, experimental data and thermodynamic; (a) fill level = 10%; (b) fill level = 30%; (c) fill level = 50%; (d) fill level = 70%.
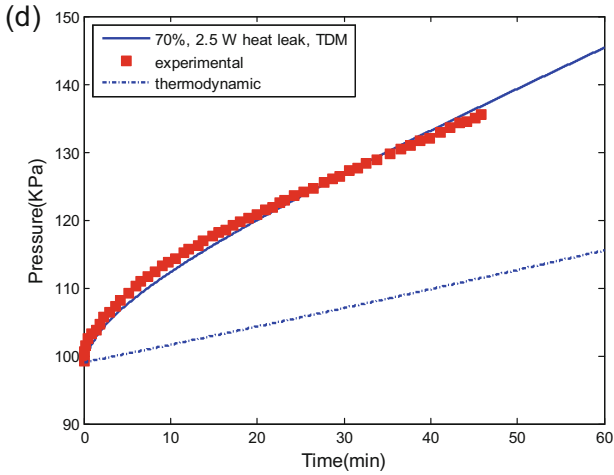
Fig. 2. (*continued*)

and experiment. For the cases of fill levels above 10%, the agreement between the TDM predictions and experiments is fine for both the rate and magnitude of the vapor rise. The rate of pressure rise is large at first period and arrives at a constant value equal to the thermodynamic predictions finally. The deviation is negative at first and positive at the end of the calculation but all with an acceptable error range. For the low fill level of 10%, TDM model does an unsatisfactory job of predicting the magnitude of the vapor pressure while captures the rise rate well as the thermodynamic. This is so because the fluid mixing more sufficient at low fill level. Thermal stratification degree is not pronounced as the high fill levels. The predicted value is lower than the experimental value because TDM ignores the convective diffusion effect before the reservoir fluid temperature reaches the same level.

Figure 3 gives the results of calculations by the described procedure and the values of the self-pressurization in a tank with liquid hydrogen experimentally obtained in the K-site facility [7, 14, 15]. The vessel was composed by a vacuum chamber enclosing a cylindrical cryoshroud. The temperatures were measured by electrical resistance heaters. The tank was covered by two MLI blankets were used to cover the tank and radiative losses were reduced. 28.08 W heat power is into the system. Relevant thermodynamic properties of fluid used in calculation model are listed in Table 2.

It is demonstrated in Fig. 3 the predictions of TDM model capture the experiment data well in fill levels of 29% and 83%. However, for the fill level 49% TDM model performs excellent at the first 6 h but after that the model's predictions becomes poor compared with experiment. It was declared by Baris and Kassemi [5] that the heating style is responsible for the deracy. It may not be the uniform heat flux boundary condition. The heat flux into liquid in TDM is

$$\dot{Q}_L = \frac{\dot{Q}}{A_{\text{wall}}} A_L = 13.86 \text{ W} \tag{22}$$

Table 2. Thermodynamic properties of liquid hydrogen

Symbol	Property	Value
ρ_L	Liquid density	70.734 kg/m^3
c_L	Liquid specific heat at constant volume	5678.2 J/kg K
c_V	Vapor specific heat at constant volume	14283 J/kg K
λ_L	Liquid thermal conductivity	0.10349 W/m K
L	Latent heat	445196.6 J/kg

where A_{wall} is the tank wall area, A_L is the tank wall area occupied by liquid Fig. 3(b). The TDM predictions exceed the experimental data means heat flux into vapor is below that heating uniformly. $\dot{Q}_V$ is

$$\dot{Q}_V = \dot{Q} - \dot{Q}_L = \frac{\dot{Q}}{A_{\text{wall}}} A_V \tag{23}$$

Where A_V is the tank wall area occupied by vapor. Therefore, $\dot{Q}_L$ is increased to 18 W with $\dot{Q}_L$ staying at 28.08 W. Figure 4(a) shows the pressure calculated by TDM matches the experimental well. In order to verify that nonuniformly heating occurred in the fill level of 49%, the experimental data under $q_w= 3.5$ W/m^2 is used for the verification. Thus $\dot{Q}_L = 31.5963$ W with the same A_L when $\dot{Q}_L = 18$ W. The agreement is obtained in Fig. 4(b). More strict and clear experimental condition plays an important role in the validation of theory prediction model. The thermodynamic model underestimates the experimental self-pressurization due to the neglection of the conduction and convection effect in the liquid. It assumes the system is homogeneous and the saturation temperature states with that corresponding to the vapor pressure.

The experiments in Fig. 2 are carried out in different fill levels for different heat leak. Therefore, it is difficult to conclude the influence of fill level on the self-pressurization. Figure 5 gives the pressure variation in different fill levels of the same heat leak of 2 W by using thermal diffusion model. The pressurization rate decreases with increasing fill level. For a fixed heat power, as liquid volume increases due to the increasing fill level, the heat capacity increases. Thus the self-pressurization rate decreases. This phenomenon is not obvious in the NASA's experiment tank. It was observed that the pressure rise rates were lowest at middle fill levels for LH2. Pressure rise rates at varying fill level are subject to the combined effects of the liquid fill level, wall area occupied by liquid, liquid-vapor interfacial area, and system heating model.

The diameter and height of the tank are increased to 1.5 times of the experimental one. The cases of equal heat leak 2 W and equal volume energy source Q/V_T are investigated at a fixed fill level of 30%. The predicting results are shown in Fig. 6. Pressure rise is decreased as tank volume increases due to the gas volume increases with the same heat
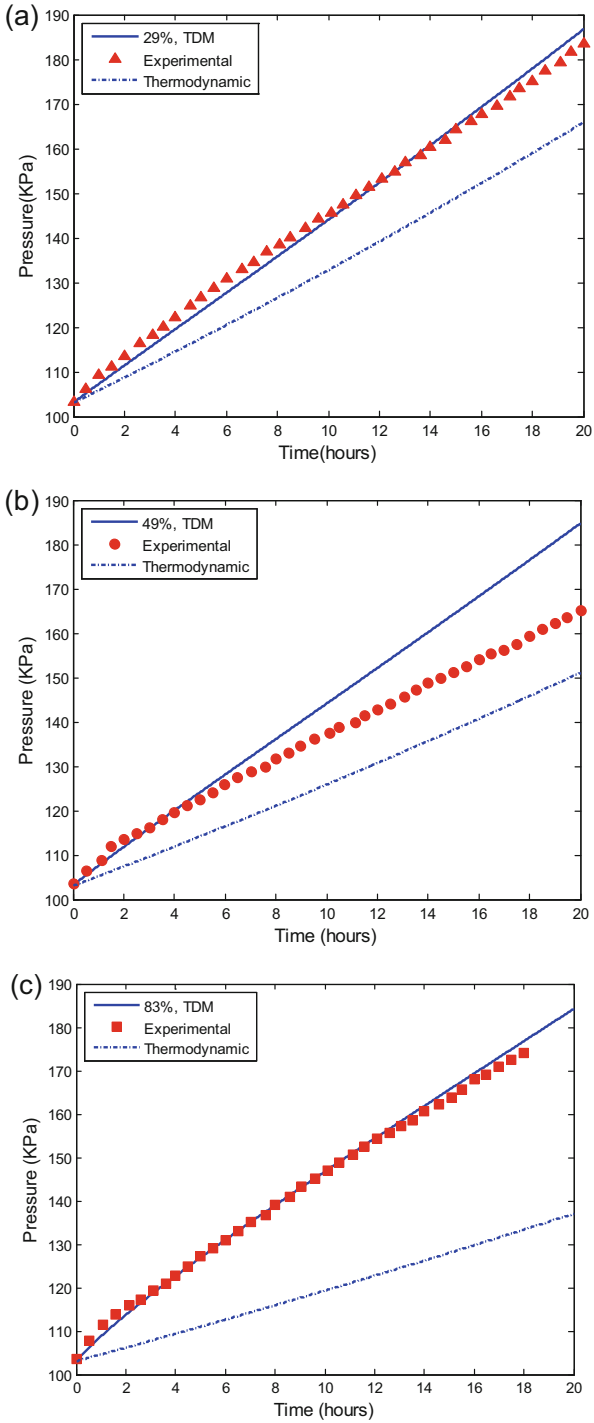
Fig. 3. Comparison of TDM, experimental data and thermodynamic; (a) fill level = 29%; (b) fill level = 49%; (c) fill level = 83%.
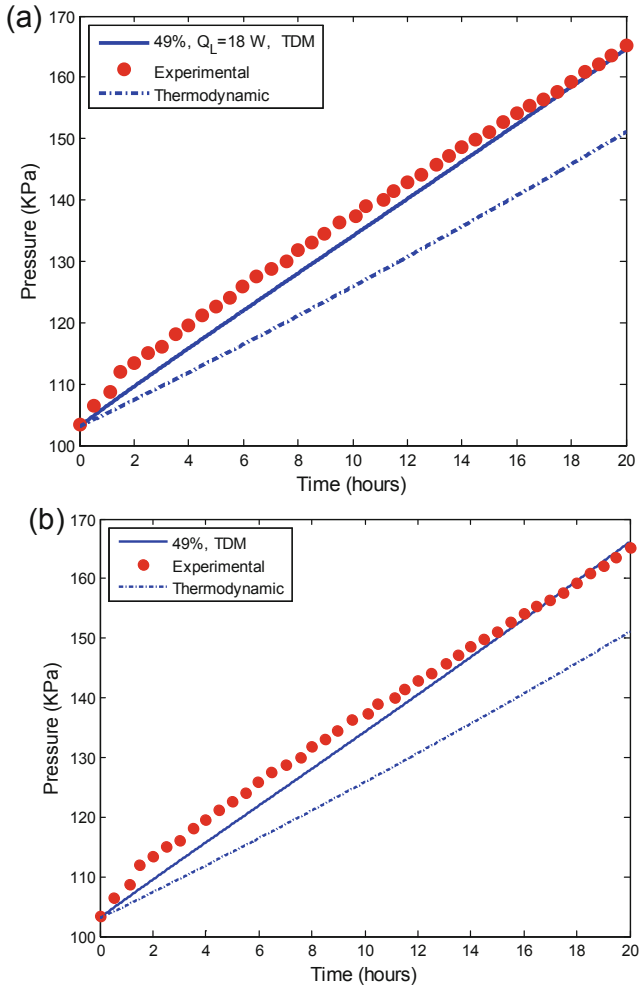
Fig. 4. Comparison of TDM, experimental data and thermodynamic of unknown heating condition (fill level = 49%).

leak. However, when the volume energy sources are equal, pressurization in the large tank increases more quickly. This is so because the interface area is larger resulting in increase of Q_{IL}.
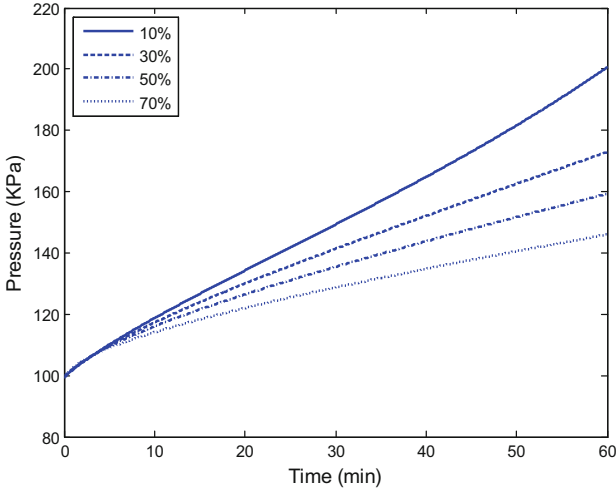
Fig. 5. Self-pressurization for different fill levels with the same heat load of $Q = 2.0$ W.
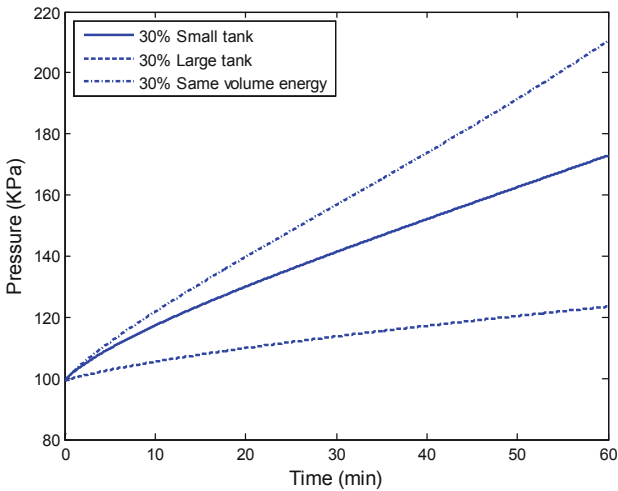
Fig. 6. Comparison of self-pressurization different tank sizes.

4   Conclusion

In this paper, a coupled thermal diffusion model is developed by employing a concentration parameter model in the vapor and a one-dimensional heat conduction model in the liquid to predict the self-pressurization in cryogenic storage tanks. The predictive capability of the model is assessed by comparing the model's predictions with cryogenic self-pressurization data obtained during experiments in Korea Advanced Institute of Science and Technology with liquid nitrogen and in NASA Glenn's K-site facility with

liquid hydrogen. Comparisons between the model predictions and experimental data are conducted and agreements are reasonably acceptable. For the cylindrical tank of liquid nitrogen, the trend is that pressurization rate is lower when the fill level increases. Pressure rise is decreased as tank volume increases due to the gas volume increases with the same heat leak. Pressurization is influenced by the heat and mass exchange at the interface for two different size tanks with equal volume energy source. For the oblate spheroidal tank geometry, the effect of fill level on pressure rise is not intuitive. It is a combination of the liquid fill level, wall area occupied by liquid, liquid-vapor interfacial area, and system heating model.

References

1. Aydelott, J.: Normal gravity self-pressurization of 9-inch (23 cm) diameter spherical liquid hydrogen tanks. NASA TND-4171(1967)
2. Hochstein, J., Ji, H.-C., Aydelott, J.: Prediction of self-pressurization rate of cryogenic propellant tankage. J. Propul. Power **6**(1), 11–17 (1990)
3. Abdalla, K., Frysinger, T., Androcchio, C.: Pressure-rise characteristics for a liquid hydrogen dewar for homogeneous, normal gravity, quiescent, and zero-gravity tests. NASA TM X-1134 (1965)
4. Amirkhanyan, N., Cherkasov, S.: Theoretical analysis and procedure for the calculation of thermophysical processes occurring in a cryogenic vessel under conditions of nonvented storage. High Temp. **39**(6), 905–911 (2001)
5. Baris, S., Kassemi, M.: Numerical and experimental comparisons of the self-pressurization behavior of an LH2 tank in normal gravity. Cryogenics **48**, 122–129 (2008)
6. Panzarella, C., Kassemi, M.: On the validity of purely thermodynamic descriptions of two phase cryogenic fluid storage. J. Fluid Mech. **484**, 41–68 (2003)
7. Dresar, N.V., Lin, C., Hasan, M.: Self-pressurization of a flightweight liquid hydrogen tank: effects of fill level at low wall heat flux. NASA TM 105411 (1992)
8. Roh, S., Son, G.: Numerical study of natural convection in a liquefied natural gas tank. J. Mech. Sci. Technol. **26**(10), 3133–3140 (2012)
9. Grayson, G., Lopez, A., Chandler, F., Hastings, L., Tucker, S.: Cryogenic tank modeling for the saturn AS-203 experiment. In: AIAA 2006-5258 (2006)
10. Das, S.P., Chakraborty, S., Dutta, P.: Studies on thermal stratification phenomenon in LH2 storage vessel. Heat Transfer Eng. **25**, 54–66 (2004)
11. Kumar, S.P., Prasad, B.V.S.S.S., Venkatarathnam, G., Ramamurthi, K., Murthy, S.S.: Influence of surface evaporation on stratification in liquid hydrogen tanks of different aspect ratios. Int. J. Hydrogen Energy **32**, 1954–1960 (2007)
12. Ren, J., Shi, J., Liu, P., Bi, M., Jia, K.: Simulation on the thermal stratification and destratifiction in liquefied gas tanks. Int. J. Hydrogen Energy **38**(10), 4017–4023 (2013)
13. Seo, M., Jeong, S.: Analysis of self-pressurization phenomenon of cryogenic fluid storage tank with thermal diffusion model. Cryogenics **50**, 549–555 (2010)
14. Stochl, R., Knoll, R.: Thermal performance of a liquid hydrogen tank multilayer insulation system at warm boundary temperatures of 630, 530, and 152 R. NASA TM 104476 (1991)
15. Hasan, M., Lin, C., Dresar, N.V.: Self-pressurization of a flightweight liquid hydrogen storage tank subjected to low heat flux. NASA TM 103804 (1991)